Experimental Investigation and High Resolution Simulator of In-Situ Combustion Processes

Quarterly Report

Start date: July 2004
End date: September 2004

Margot Gerritsen
Anthony R. Kovscek

October 2004

DE-FC26-03 NT15405

Department of Petroleum Engineering
Stanford University
Green Earth Sciences Building
367 Panama Street
Stanford, CA 94305-2220

Abstract

Accurate simulation of in-situ combustion processes is computationally very challenging because the spatial and temporal scales over which the combustion process takes place are very small. In this third quarterly report of our DoE funded research, we continue the discussion of the design of a new simulation tool based on an efficient Cartesian Adaptive Mesh Refinement technique that allows much higher grid densities to be used near typical fronts than current simulators. Also, we discuss the possibility of using Strang splitting for handling the large disparity in time-scales between the kinetics and transport in the in-situ combustion process. On the experimental side, we show results of experiments with our scanning electron microscope (SEM) to investigate the sand-clay-salt mixtures that are used for combustion in which we focus on grain sizes, shapes, orientations, characteristic inter-structures, and element analysis. SEM is shown to be a very effective tool in studying these mixtures.

October 2004

Table of Contents

List of graphical materials

1. Introduction

In-situ combustion, or air injection, is the process of injecting oxygen into oil reservoirs to oxidize the heaviest components of the crude oil and enhance oil recovery through the heat and pressure produced. The emphasis of this work is to study and model numerically in situ combustion processes. The ultimate objectives are to provide a working accurate, parallel in situ combustion numerical simulator and to better understand the in-situ combustion process when using metallic additives and/or solvents combined with in situ combustion. For this purpose, experimental, analytical and numerical studies are conducted.

This report presents results of the fourth quarter of the first year of this project.

2. Executive Summary

2.1. Personnel

Current personnel include Prof. Margot Gerritsen (PI), Prof. Tony Kovscek (Co-PI), Dr. Louis Castanier (Technical manager), Dr. Jonas Nilsson (postdoctoral fellow), Mr. Rami Younis (PhD student) and Mr. Qing Chen (MSc student). Qing Chen replaced Binjian who graduated in June 2004. His MSc report will be send to DoE separately.

2.2. Important accomplishments

2.2.1 Towards a split-step, factored framework

In the previous quarterly report, we mentioned that we are seeking an efficient solution method for the transport equations (that involve very fast kinetic reactions) using Strang splitting. This technique splits the kinetic equations from the transport equations, allowing for a more efficient transport solve. A separate system of ordinary differential equations is solved for the kinetics. We are investigating efficient proxies for its calculation.
In the previous reports we described our one-dimensional in-situ combustion simulator. This simulator is currently being upgraded to allow for faster nonlinear solves using the PETSc solver package. This simulator will be extended in the coming year to experiment with the splitting methods.

Numerical splitting techniques are essentially factored forms of numerical operators. They have been extensively used in other areas such as CFD, where for example, they are applied to reducing multi-dimensional problems into a sequence of simpler one-dimensional problems (e.g. ADI methods), to treating problems with more than one physical mechanism of transport with appropriate schemes for each mode independently, and to coupling combustion kinetics to transport in open-air combustion.

The development of a split-step method for the ISC process has the potential to address the following points:

- Separation of scales. The splitting allows the integration of chemical reactions to occur over a finer sampling than a single step for flow or transport, leading to a more efficient treatment of the sources of stiffness.
- Specialized numerical schemes to treat different processes. For example diffusion and advection terms appearing in the same equation can be treated independently and then combined.
- Projection methods which could allow one part of say pressure to be solved at each time-step followed by a correction of another part attributed to change in chemistry over the time-step.

First, we give a brief summary of factored methods, followed by a highlight of the forms specialized to ISC that will be studied, and finally, by a summary of the most important considerations to analyzed.

Factored forms

The concept is illustrated by a simple example. Consider the problem time-dependent problem below, where the matrices A and B represent spatially discretized operators.

$$\frac{d\vec{u}}{dt} = (A+B)\vec{u}$$

Now suppose we use a simple explicit scheme written as below.

$$U^{n+1} = (I + hA + hB)U^n + \mathrm{O}(h^2)$$

A factored form can be derived readily and is given as the first term on the right hand side of the following equation. Clearly, the difference to the unfactored form is of the same order as the truncation error.

$$U^{n+1} = (I + hA)(I + hB)U^n - (h^2 AB)U^n + \mathrm{O}(h^2)$$

Dropping the second term on the right hand side (that is, accepting that it is of the order of the truncation error) we can solve the factored form below instead.

$$W^{n+1} = (I + hB)U^n$$
$$U^{n+1} = (I + hA)W^{n+1}$$

The factored and unfactored forms may have very different properties, in terms of computational cost for set-up and solver time, as well as in many cases, stability. These differences can be exploited to generate a more efficient solver. Factored forms can also be applied to implicit methods. For example, consider the weighted implicit scheme below,

$$\frac{U^{n+1} - U^n}{h} = A\left[\theta U^n + (1-\theta)U^{n+1}\right] + B\left[\omega U^n + (1-\omega)U^{n+1}\right]$$

This scheme has the factored form below, which gives rise to a four step scheme.

$$\left[I - h(1-\theta)A\right]\left[I - h(1-\omega)B\right]U^{n+1} = \left[I + h\theta A\right]\left[I + h\omega B\right]U^n$$

$$U_{n+1}^{(1)} = \left[I + h\omega B\right]U^n$$
$$U_{n+1}^{(2)} = \left[I + h\theta A\right]U_{n+1}^{(1)}$$
$$U_{n+1}^{(3)} = \left[I - h(1-\theta)A\right]^{-1} U_{n+1}^{(2)}$$
$$U_{n+1}^{(4)} = \left[I - h(1-\omega)B\right]^{-1} U_{n+1}^{(3)}$$

The Strang splitting that we introduced in the last quarterly report is a special factorization that is similar to the case where θ=1 and ω=1/2, except that the B operator is applied over a half time step, followed by the A operator over a full step, and finally, by the B operator once again, over a half step. So,

$$U_{n+1/2}^{(1)} = \left[I + h\omega B\right]U^{n}$$
$$U_{n+1}^{(2)} = \left[I + h\theta A\right]U_{n+1/2}^{(1)}$$
$$U_{n+1}^{(3)} = \left[I + h\omega B\right]U_{n+1}^{(2)}$$

The above examples are all for simple, illustrative linear problems, but the ideas are extensible to more complex nonlinear cases.

Re-cast of the ISC equations

Extending the notation introduced in previous reports, we can introduce the following variables,

$$C_i^p = \rho^p X_i^p$$
$$U^p = \rho^p e^p$$
$$H^p = \rho^p h^p$$

We now re-formulate the ISC equations whilst neglecting gravity and capillary pressure to help make the formulation more clear. First, total flow conservation along with Darcy's law is arrived at by summing all mass conservation equations. This results in

$$u_T = -k\lambda_T \nabla p$$
$$\frac{\partial}{\partial t}\left(\phi_f \sum_p S^p \rho^p\right) + \nabla\left(u_T \sum_p \rho^p\right) + \sum_{i,p} Q_{i,well}^p = 0$$

Next, we retain Nc-1 species mass conservation equations but cast them in terms of fractional flows in the form

$$i \in \{1,\ldots,Nc-1\};$$
$$\frac{\partial}{\partial t}\left(\phi_f \sum_p S^p C_i^p\right) + \nabla\left(u_T \sum_p f^p C_i^p\right) + Q_{i,rx} + \sum_p Q_{i,well}^p = 0$$

Finally, the heat equation is also written in terms of the variables defined above, which gives

$$\frac{\partial}{\partial t}\left(\phi_f \sum_p S^p U^p\right) + \nabla\left(u_T \sum_p f^p H^p\right) + \nabla\left(K_T \nabla T\right) + H_{rx} + H_{wells} = 0$$

Deriving useful factored forms for the ISC equations

Combining ideas from the previous two sections, we note that

- Darcy's law along with the total flow conservation equation can, as is generally done, be aligned with pressure. However, numerically we can treat total pressure as the sum of two components, where one component is solved for using the current equations, and the other component is treated as a correction due to the transport.
- The species conservation equations are hyperbolic, and here we have two physical operators. In analogy to the discussion in the previous sections, we can represent the advection by A and the reaction by B. Hence a direct application of the splitting is to solve the advection, and the system of reaction ODE for concentrations and saturations in a segregated manner.
- The heat equation couples three physical processes; conduction, convection, and reaction. Aligning the heat equation with temperature, and splitting conduction from convection, we can apply another factored form, if this leads to improvements in efficiency.

Overall, we plan to split both pressure and temperature in two components. We start by solving for one, followed by an inner splitting for the saturations and concentrations (reaction and advection), followed by a final correction procedure to account for the second component of the pressure and temperature. An example procedure would be to

I. Solve the pressure equation for one time-step with explicit temperature, saturations, and concentrations.
    1. Solve for new temperature using old saturations, and concentrations on a factored form with no reactions
    2. Solve for saturations and concentrations using new pressures
        a. Solve the system of reaction equations on a half step, and update concentration/saturation initial conditions for next step
        b. Solve a full step for the advection system. Update initial conditions for next step.
        c. Solve the system of reactions on a second half-time-step
    3. Perform a temperature correction using reaction rates obtained, and factored form with conduction

II. Revise pressure estimate by a for example requiring a zero residual for the water saturation equation.

In-Situ Adaptive Tabulation (ISAT)

In solving the system of Ordinary Differential Equations (ODEs) for the kinetics, we may apply the ISAT idea to avoid direct integration for large number of components. Studying Singer and Pope 2003 [1], direct application of the ISAT code would be possible. By defining the concentrations as primary variables, rather than fractions, and by freezing the thermodynamic state variables P, and T, the reaction operator becomes similar to their model problem, with the exception of the nonlinearity. We need to further investigate this approach and estimate its accuracy and computational benefit.

2.2.2 The three dimensional adaptive pressure solver

The compact control-volume finite difference formulation for the discretization of the homogeneous pressure equation has been tested. In order to obtain an accurate method, the fluxes are computed by a three point finite difference approximation. The anisotropic refinements

require the three point stencil to be combined with a cubic interpolation of the cell centered pressure values in the adjacent cells.

We have compared the solution of the discretized pressure equation on the anisotropic grids with the standard two-point discretization on a uniform grid for a 3D problem with a forced solution. The maximum errors as a function of the number of grid cells for both uniform refinements and anisotropic refinements are shown in Table 1. It clearly shows the benefit of adaptive refinement.

UNIFORM GRID	
Number of cells	Maximum Error
4096	0.26
32768	0.34
Adaptive Mesh Refinement	
Number of cells	Maximum Error
200	0.367
1600	0.069
12800	0.028
102400	0.007

Table 2: Comparison of maximum errors for uniform and adaptive rectangular refinement.

We have also performed comparisons between fine uniform pressure solutions and pressure solutions on an adaptive grid where we in both cases use a saturation profile as our mobility field in the pressure equation. The top image in Figure 1 (a) shows the saturation profile, and the two following images are the pressure solutions on a fine uniform grid (b) and an anisotropic adaptive grid (c), respectively. We achieve a reasonable accurate solution for the adaptive mesh using only 2099 grid cells, compared to the fine grid solution with 16384 grid cells. A similar result is achieved with the saturation profile shown in Figure 2 (a). In these computations we had the same resolution on the fine uniform grid but only 1875 grid cells in the adaptive mesh.

The extension to heterogeneity is in progress. We have implemented a pressure discretization for elimination of adaptive isotropic interface errors, proposed by Edwards [2]. The discretization has been generalized to also fit the anisotropic grids we are using. We are in the process of implementing a novel higher-order discretization. The adaptive meshes also require a tailored upscaling technique to get relevant permeabilities at the various grid scales. We will discuss this technique in later quarterly reports.

2.2.2 Experimental in-situ combustion

In previous quarterly reports, detailed experiments were conducted in a kinetics cell to understand the rates and kinetics of in-situ combustion. These experiments contrasted the combustion performance of a number of crude oils in the presence and absence of tin chloride ($SnCl_2$) and iron nitrate ($Fe_2(NO3)_3$). Water-soluble, metallic additives such as these improve combustion by affecting cracking, low temperature oxidation, and pyrolysis reactions thereby improving fuel laydown. The mechanism of catalysis by metalic additives is not yet known. It is our working hypothesis, however, that the cationic metals ion exchange with ions residing in the clay to create

an activated site that acts in a manner analogous to a heterogeneous catalyst. Developing a mechanistic understanding is one key to improve and expand application of in-situ combustion. Accordingly, an experimental investigation is underway to test the above hypothesis. The setup is described in section 3 of this report. This investigation is still subject to further interpretation. The following observations have, nonetheless, emerged. First, the introduction of metallic catalyst ions has not changed remarkably the morphology of the clay within mixtures of sand and clay. Figure 3 contains a representative result that contrasts the clay structure in the absence and presence of the ion Fe^{3+}. Images are at 1000X magnification and note the horizontal bar illustrating a dimension of 10 μm. Figure 4 presents views of the same systems at 4000x. Again, note the horizontal bar indicating a size of 5 μm. Figure 4(b) may illustrate a greater fraction of clay agglomerations that are roughly 1 μm is size. Nevertheless, at these two scales, clay morphology is remarkably similar in the presence or absence of aqueous metallic additives.

A second aspect of the investigation is to obtain information about the location of metal ions on the solid substrate. Our past kinetics cell experiments have used both sand and kaolinite as well as sand and amorphous silica powder. Hence, these same systems were examined with the SEM. At first glance, attempting to determine the location of metal ions on the solid substrate is akin to searching for a needle in a haystack. Various probes available for the SEM have aided in the search. Figure 5 illustrates a localized deposit of iron (Fe^{3+}) on what appears to be a quartz sand grain at 1400X. The inset shows the iron deposit at 6000X. The identification of iron was verified by the elemental analysis provided by EDS. The remainder of material in this view is the silica powder. Figure 6 presents results from the system sand-kaolinite-tin chloride. The composition of the region in the SEM image marked by a square is given in the spectrum below the image. The size, shape, and elemental composition (Al, Si, O) of the solid material in the figure indicate that is clay. The remarkable (and happy) aspect is the relatively high abundance of tin (Sn) within the square. It appears quite likely that tin has participated in cation exchange and is emplaced within the clay.

3. Experimental

The experimental investigation makes use of scanning electron microscopy (SEM) and elemental dispersive X-ray spectroscopy (EDS) to gauge any morphological changes in clay structure and to locate (if possible) the location of the metal catalyst within the mixes of sand, clay, fine amorphous silica powder, and metallic additives that are used for combustion experiments. In brief, various mixtures that are representative of the solid substrates and ionic environment of combustion experiments were prepared (for instance sand-kaolinite-1wt% $Fe(NO3)_3$ solution or sand-silica powder) and dried under vacuum. Mounts of these various mixtures were prepared for observation in the SEM. All samples are sputtered with a gold-palladium mixture to improve surface conductivity thereby enhancing image quality.

4. Results and discussion

This report covers the fourth quarter of our research grant. The quarter was used primarily to further design the computational algorithms, with increased emphasis on the three-dimensional simulator, and to continue our experimental work. We have made very good progress in these areas again this quarter. Our abstracts on the work to the Society of Petroleum Engineers Reservoir Simulation Symposium, to be held early 2005, and the Society of Petroleum Engineers

Western Regional Meeting in March 2005, were both accepted and we are in the process of preparing the papers.

Numerical simulations – transport and kinetics

We have investigated the potential use of Strang splitting to reduce the extreme stiffness introduced by the reaction equations in our numerical model. Strang splitting has been used successfully in open-air combustion [1]. In-situ combustion processes have a larger disparity in scales, both in time and space. Also, there is added sensitivity in the equations to phase behavior as opposed to open-air combustion. Both require adaptation of the methods proposed in [1]. It is too early to conclude that this approach will be successful, but we are very optimistic. We will focus on this development stronger in the second year of our grant.

Further tests of the anisotropic Cartesian adaptive gridding technique has shown the robustness and efficiency of this method. We have implemented an extension to heterogeneous media, and are currently investigating appropriate upscaling techniques for the anisotropic grids.

Experimental work

Our experiments this quarter have shown that the introduction of metallic catalyst ions does not change remarkably the morphology of the clay within mixtures of sand and clay. A second aspect of the investigation is to obtain information about the location of metal ions on the solid substrate. We were happy to find a strong likelihood that tin has participated in cation exchange and is emplaced within the clay.
The results given in Figs. 5 and 6 are in agreement with the working hypothesis, described in section 2, that metallic ions create activated sites within the solid substrate where combustion processes are enhanced. Moreover, mixtures of sand, clay (or silica powder), and water soluble, metal ions displayed greatest oxygen consumption, and optimum combustion characteristics during kinetics cell experiments in direct correspondence to the visual observations made this quarter.

5. Conclusions

We have nearly finished the development of the three-dimensional flow solver for incompressible flows using anisotropic refined grids in heterogeneous media. Although it is too early to conclude that our approach is entirely successful, early indications are that the proposed methodology will improve both robustness and efficiency of the pressure solver. Our next step will be to extend the methodology to compressible cases. We expect this to be finished before the end of the second year of our grant.

On the experimental side, we will continue to focus on understanding how the additives work during combustion. Our work this quarter, highlighted by the results shown in Figs. 5 and 6, seem to confirm the working hypothesis that metallic ions create activated sites within the solid substrate where combustion processes are enhanced. Moreover, mixtures of sand, clay (or silica powder), and water soluble, metal ions displayed greatest oxygen consumption, and optimum combustion characteristics during kinetics cell experiments in direct correspondence to the visual observations made this quarter. The current results are a step forward to improving the design of in-situ combustion processes using metallic additives.

References

[1] M. A. Singer and S. B. Pope., Exploiting ISAT to Solve the Equations of Reacting Flow, 2003.

[2] M. G. Edwards, Elimination of Adaptive Grid Interface Errors in the Discrete Cell Centered Pressure Equation, *J Comput. Phys.*, 126 (1996), 356-372.

[3] Chen, Y., Durlofsky, L.J., Gerritsen, M., Wen, X.H., A Coupled Local-Global Upscaling Approach for Simulating Flow in Highly Heterogeneous Formations, Advances in Water Resources, 26, 1041--1060, 2003.

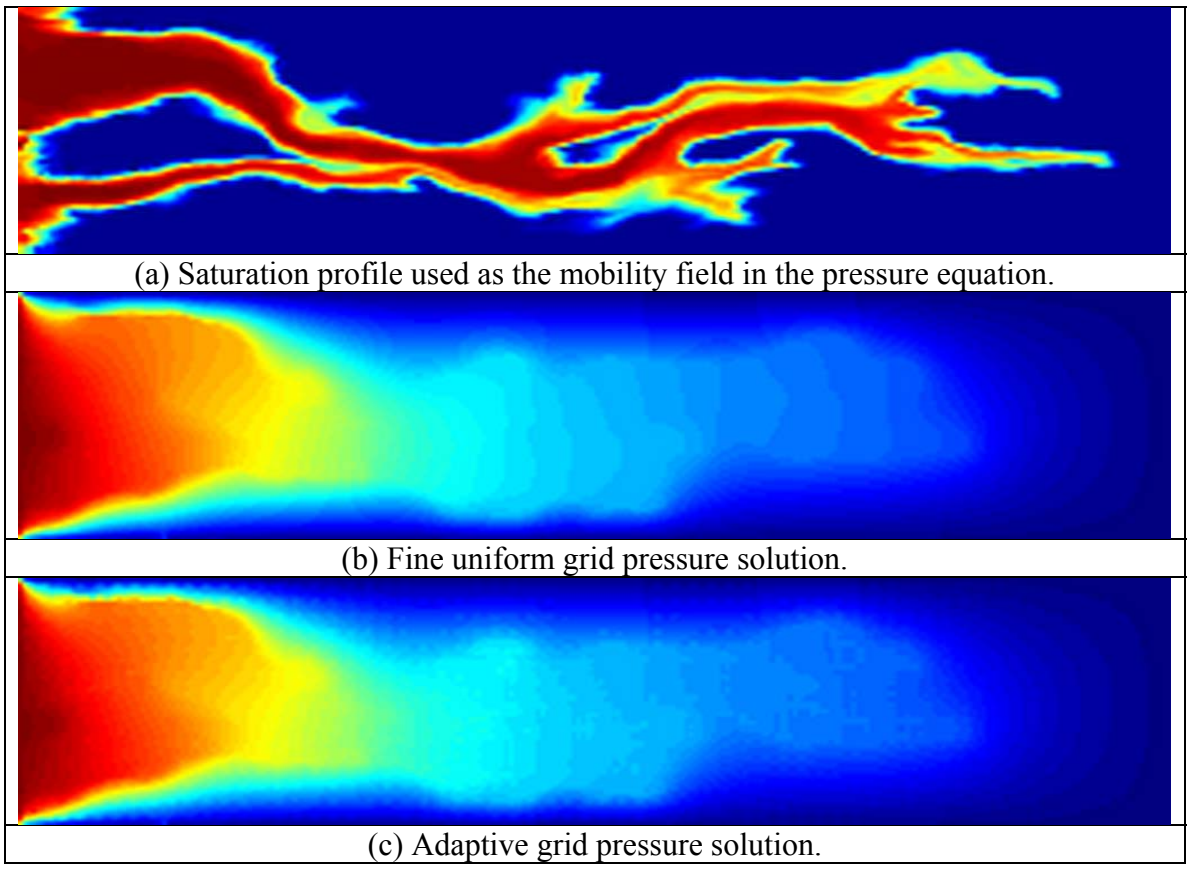

(a) Saturation profile used as the mobility field in the pressure equation.

(b) Fine uniform grid pressure solution.

(c) Adaptive grid pressure solution.

Figure 1: Comparison between fine uniform and adaptive pressure solution based on a saturation profile.

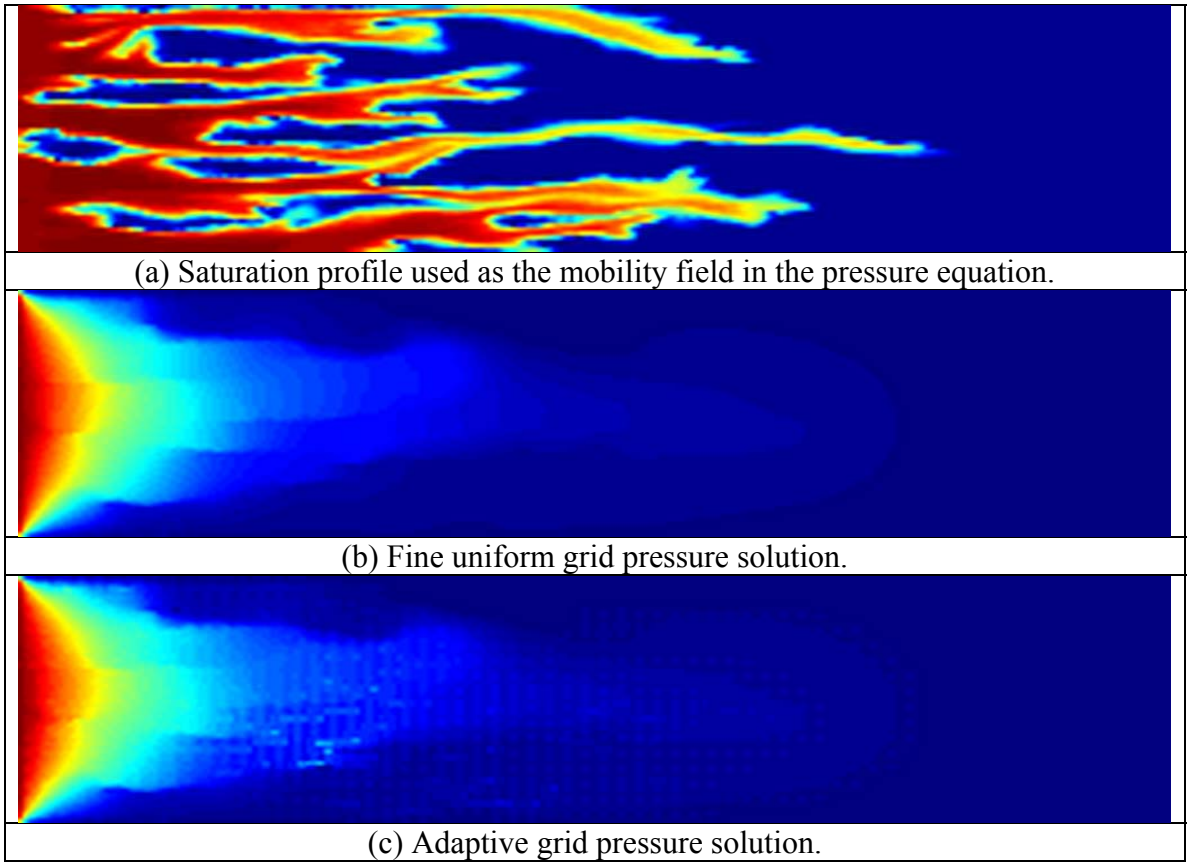

(a) Saturation profile used as the mobility field in the pressure equation.

(b) Fine uniform grid pressure solution.

(c) Adaptive grid pressure solution.

Figure 3: Comparison between fine uniform and adaptive pressure solution based on a saturation profile.

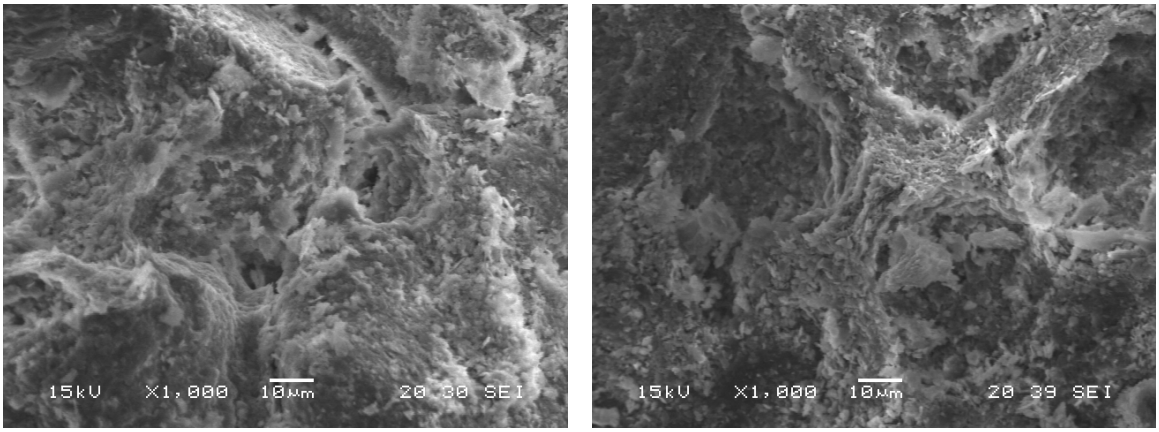

(a) (b)

Figure 3. (a) Mixture of sand and kaolinite and (b) mixture of sand, kaolinite, and Fe^{3+}.

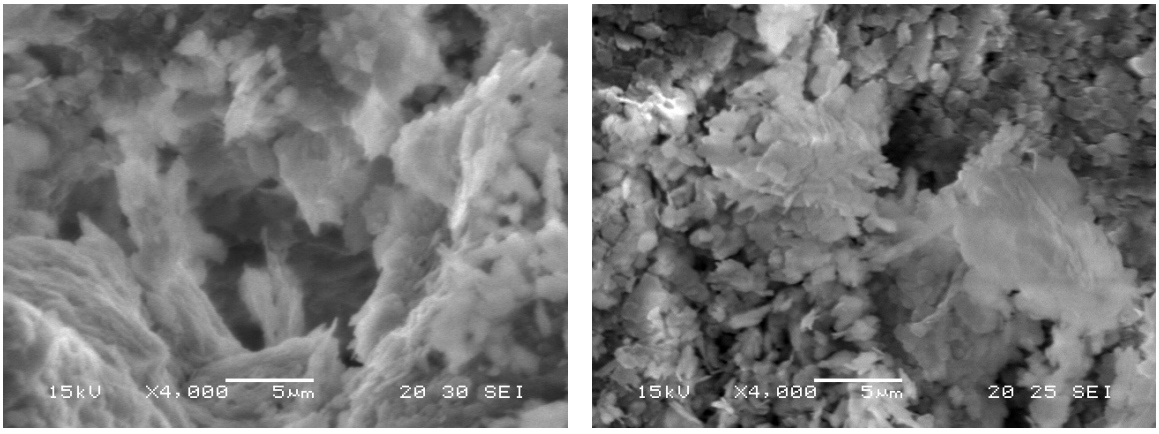

(a) (b)

Figure 4 (a) Mixture of sand and kaolinite and (b) mixture of sand, kaolinite, and iron (Fe)

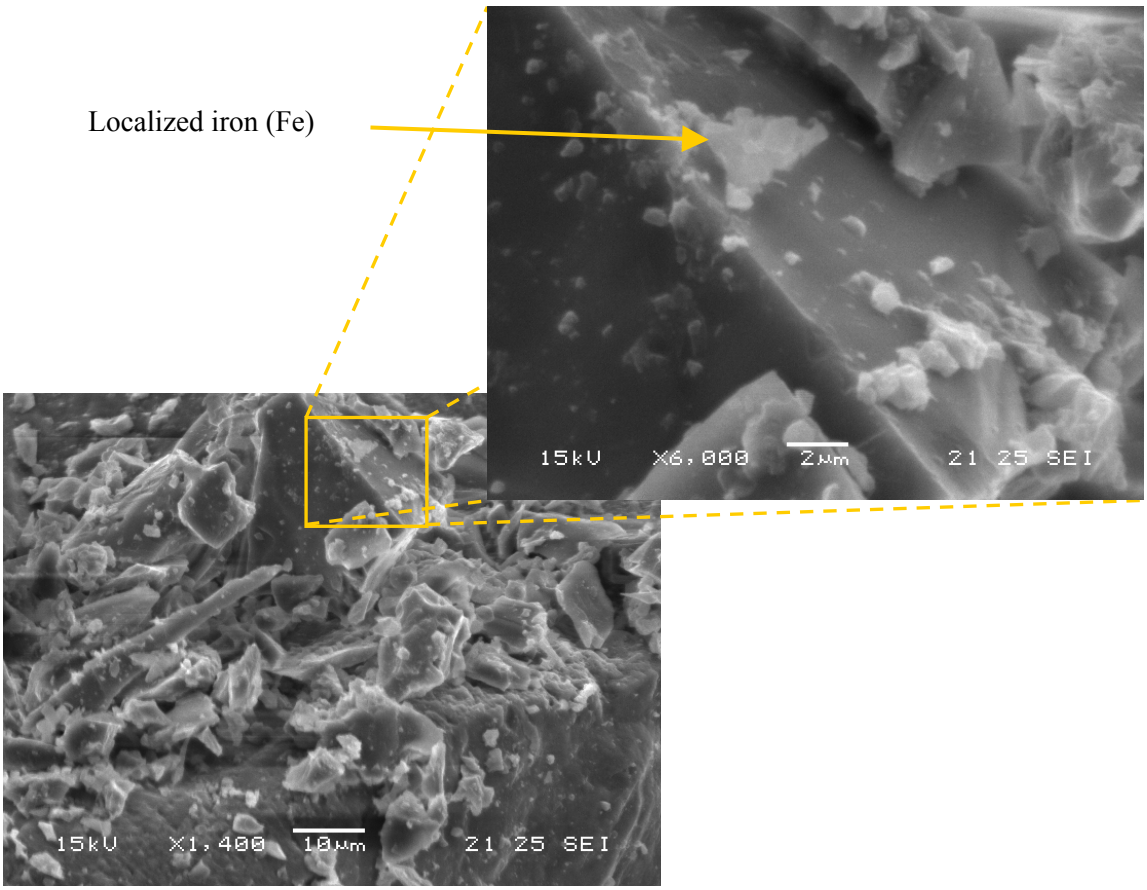

Figure 5 Mixture of sand, amorphous silica powder, and iron (Fe)

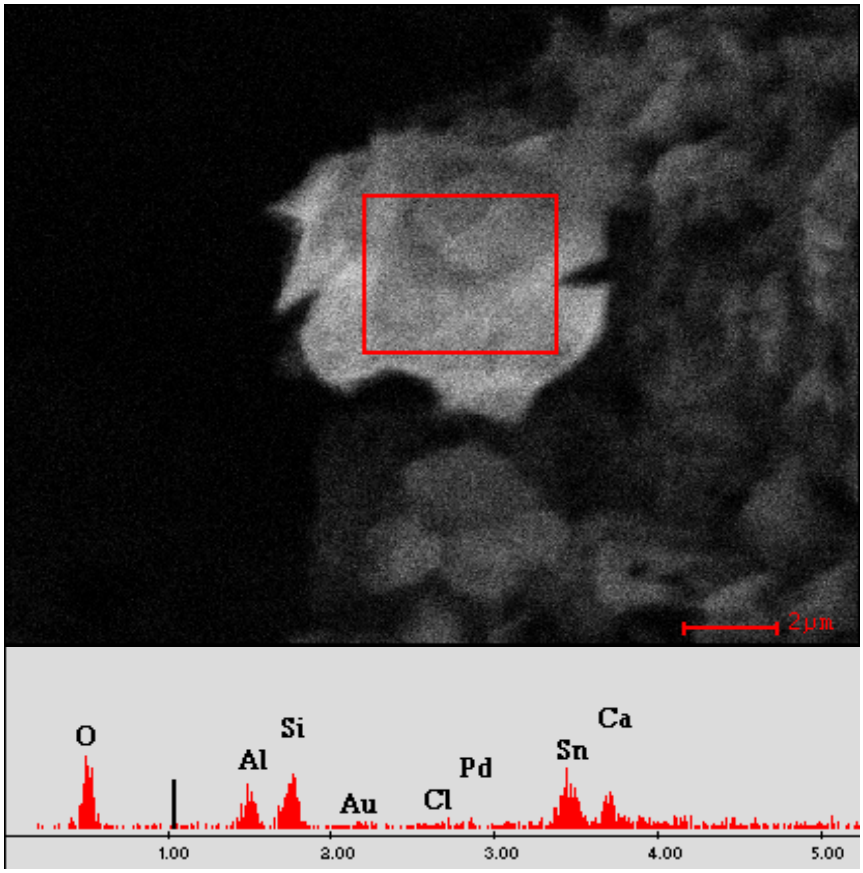

Figure 6 Localized tin in mixture of sand, kaolinite, and tin (Sn)